Published in final edited form as:
J Mol Cell Cardiol. 2010 January ; 48(1): 238. doi:10.1016/j.yjmcc.2009.05.014.

Connexin40 and Connexin43 Determine Gating Properties of Atrial Gap Junction Channels

Xianming Lin[1], **Joanna Gemel**[3], **Aaron Glass**[2], **Christian W. Zemlin**[1], **Eric C. Beyer**[3], and **Richard D. Veenstra**[1]

[1]Department of Pharmacology, SUNY Upstate Medical University, Syracuse, NY 13210

[2]Dept of Microbiology and Immunology, SUNY Upstate Medical Univ., Syracuse, NY 13210

[3]Department of Pediatrics, University of Chicago, Chicago, IL 60637

Abstract

While ventricular gap junctions contain only Cx43, atrial gap junctions contain both Cx40 and Cx43; yet the functional consequences of this co-expression remain poorly understood. We quantitated the expression of Cx40 and Cx43 and their contributions to atrial gap junctional conductance (g_j). Neonatal murine atrial myocytes showed similar abundances of Cx40 and Cx43 proteins, while ventricular myocytes contained at least 20 times more Cx43 than Cx40. Since Cx40 gap junction channels are blocked by 2 mM spermine while Cx43 channels are unaffected, we used spermine block as a functional dual whole cell patch clamp assay to determine Cx40 contributions to cardiac g_j. Slightly more than half of atrial g_j and ≤20% of ventricular g_j were inhibited. In myocytes from Cx40 null mice, the inhibition of ventricular g_j was completely abolished, and the block of atrial g_j was reduced to < 20%. Compared to ventricular gap junctions, the transjunctional voltage (V_j)-dependent inactivation of atrial g_j was reduced and kinetically slowed, while the V_j-dependence of fast and slow inactivation was unchanged. We conclude that Cx40 and Cx43 are equally abundant in atrium and make similar contributions to atrial g_j. Co-expression of Cx40 accounts for most, but not all, of the differences in the V_j-dependent gating properties between atrium and ventricle that may play a role in the genesis of slow myocardial conduction and arrhythmias.

Keywords

atrium; ventricle; gap junctions; connexin43; connexin40; spermine

INTRODUCTION

Gap junction channels are critical for the propagation of electrical conduction in the myocardium [1]. The atrial myocardium is distinct from the ventricular myocardium in its morphologic, contractile, and electrophysiological properties. Among the differences between these tissues are their repertoires of gap junction subunit protein (connexin, Cx) expression. While four connexins (mCx30.2/hCx31.9, Cx40, Cx43, and Cx45) have been identified within

Corresponding Author: Richard D. Veenstra, Ph.D. Department of Pharmacology SUNY Upstate Medical University 750 East Adams Street Syracuse, NY 13210 Phone: 315-464-5145 Fax: 315-464-8014 E-mail: veenstrr@upstate.edu.

the heart, immunostaining studies suggest that Cx40 and Cx43 are the most abundant within the areas of working myocardium [2-4]. Cx43 is abundantly in gap junctions between both atrial and ventricular myocytes, while Cx40 is found only in atrial gap junctions.

Understanding the behavior of Cx40 as well as Cx43 may be important for elucidating normal atrial conduction and its disturbances. Certain forms of idiopathic atrial fibrillation have been associated with polymorphisms [5] or somatic mutations of Cx40 [6]. The Cx40 polymorphisms (within the promoter region) are also linked to a rare form of atrial standstill when combined with a loss-of-function cardiac sodium channel mutation [7]. Targeted gene deletion of Cx40 in mice produced multiple aberrations: P wave and PQ interval prolongation, prolonged sinus-node-recovery time, prolonged Wenckebach period, burst-pacing induced atrial tachyarrhythmias, reduced atrial, A-V node, and left bundle branch conduction velocity, right bundle branch block, and, paradoxically, reduced interatrial conduction heterogeneity [8-12]. In the ventricle, the heterogeneous loss of Cx43 gap junctions in a murine conditional cardiac Cx43 knockout model best exemplifies how the focal loss of cardiac gap junctions leads to significant dispersion of conduction, increased incidence of spontaneous arrhythmias, and loss of ventricular systolic function with only minor reductions in overall Cx43 expression [13,14]. The gating of Cx43-containing ventricular gap junctions during the action potential is also proposed to promote cardiac arrhythmias via inactivation and recovery that depends on transjunctional voltage (V_j) and contributes to conduction slowing or block and the formation of reentrant arrhythmias [15,16]. Despite the knowledge that reductions in functional connexin expression increase the dispersion of refractoriness and increase myocardial susceptibility to fibrillation, the functional consequences upon gap junction channel gating of Cx40 co-expression with Cx43 have not been examined in detail.

In this study, we quantified Cx43 and Cx40 expression levels and assessed the functional contribution of each connexin to the functional atrial gap junctional conductance (g_j) using the dual whole cell patch clamp technique. We used a spermine block assay to assess the functional contribution of Cx40 to cardiac g_j by comparing the amount of block between wild-type (wt) and Cx40 knockout (Cx40KO) cardiomyocytes. We also investigated the dynamic gating properties of mouse atrial gap junctions in a manner analogous to our previous studies of neonatal murine ventricular gap junctions [15].

METHODS

N2a Cell Culture

Stable transfectants of mouse Neuro2a (N2a) cells with rat Cx40 or Cx43 have previously been described [19,20]. For transient transfections, communication-deficient N2a cells were transfected with 1 μg of murine Cx45 in pTracer-CMV2 with Lipofectamine2000 according to manufacturer's instructions (Invitrogen). Green fluorescent protein (GFP) positive N2a cell pairs were identified under epifluorescent illumination on the stage of an Olympus IMT-2 inverted phase-contrast microscope with 470 nm excitation and >500 nm emission wavelengths and patch clamped [21].

Myocyte Cell Culture

Newborn C57Bl/6 mice were anesthetized with 2.5% isoflurane and the hearts excised in accordance with procedures approved by the institution's Committee for the Humane Use of Animals. The atria and ventricles were dissociated separately in a Ca^{2+}- and Mg^{2+}-free collagenase dissociation solution and the supernatant collected as described [15,16]. The primary cell cultures were enriched for cardiomyocytes by differential cell adhesion and plated onto 35 mm culture dishes at low density for electrophysiological examination or higher density

for immunoblotting 48-72 hrs later. Immunofluorescence samples were cultured on 18 mm glass coverslips coated with 10 μg/ml fibronectin in a 12-well plate.

Electrophysiology

Whole cell gap junction currents were recorded during repeated voltage clamp pulses with ventricular action potential waveforms as previously described [15,22]. Quantitative junctional voltage correction methods were used to correct for series resistance errors resulting from each patch electrode according to the expression [23]:

$$g_j = \frac{-\Delta I_2}{V_1 - (I_1 \cdot R_{el1}) - V_2 + (I_2 \cdot R_{el2})}. \quad \text{Eq. 1}$$

Simulated atrial action potential waveforms were also generated using the canine atrial action potential model of Ramirez et al. [24] and used to voltage clamp neonatal atrial cardiomyocyte gap junctions. Steady state V_j-dependent inactivation (increasing V_j) and recovery (decreasing V_j) normalized junctional conductance – voltage ($G_j - V_j$) curves were obtained using a 200 ms/mV voltage ramp protocol and fit with a Boltzmann distribution [15,16] (see Supplemental Material). Final graphs were prepared using Origin version 7.5 software (OriginLab Corporation, Northampton, MA).

Immunohistochemistry

The myocyte cell cultures were fixed and indirectly immunolabeled with connexin-specific antibodies according to the procedures of Kwong et al. [25]. Confocal fluorescence micrographs were acquired using the Zeiss LSM 510 META confocal microscope core facility and viewed using the Zeiss LSM Image Browser V3.5 software.

Immunoblot Analysis

Cell and tissue homogenates were prepared using a modification of the methods described by Gong et al. [26]. Aliquots containing 1 - 30 μg of protein were separated by SDS-PAGE on 10% polyacrylamide gels and blotted onto Immobilon-P membranes (Millipore, Bedford, MA). Membranes were blocked in 10% nonfat milk in Tris-buffered saline (TBS), incubated with rabbit polyclonal antibodies directed against carboxy-terminal domains of Cx43 or Cx40, rinsed repeatedly in TBS, and then reacted with peroxidase conjugated goat anti-rabbit IgG antibodies (Jackson ImmunoResearch Laboratories, Inc.). Immunoblots were developed with ECL Plus chemifluorescent reagents (GE Healthcare) and quantified using a STORM Phosphoimager. The abundance of connexin proteins in cell or tissue homogenates was determined by comparison of the intensity of their bands to standard curves obtained by immunoblotting dilutions of bacterially expressed fusion proteins containing the carboxyl terminal tail domains of Cx40 or Cx43 (Supplemental Fig. S1).

Real-Time PCR Analysis

Cellular RNA was extracted with TRIzol®, quantified by UV absorption, and 0.1 μg of reverse-transcribed cDNA was combined with custom forward and reverse murine Cx40 and Cx43 primers, Superscript® enzyme mix, and SYBR® GreenER™ dye in a 200 μl PCR tube (reaction volume = 25 μl). The samples were run for 40 cycles in a 96 well plate Bio-Rad iCycler® located in the qPCR Core facility, Department of Microbiology, SUNY Upstate Medical University. All results are expressed relative to GAPDH. A cellular RNA sample without reverse transcription was run as a negative control to test for genomic DNA. CT (cycle time) values were determined by the apparatus and the quality of the PCR product was confirmed by analyzing the melt-curve. Please note that lower CT values indicate a stronger

RNA signal. The difference in the CT values for Cx40 and Cx43 relative to GAPDH are provided as dCT (deltaCT) values. Relative connexin RNA expression levels were calculated based on equation:

$$\text{RNA level} = 2^{-[\text{dCT(sample)} - \text{dCT(Atrial Cx43)}]}$$

which assumes that the product amount doubles with each PCR cycle.

RESULTS

Connexin Expression and Distribution

To determine the connexin content of the mouse cardiac myocytes, we examined isolated/cultured myocytes by double label immunofluorescence microscopy (Fig. 1). Pairs of neonatal mouse atrial myocytes showed bright staining at appositional membranes using either anti-Cx40 or anti-Cx43 antibodies (Fig. 1 A, B), and the immunoreactivity substantially coincided (Fig. 1D). Confocal microscopy confirmed that Cx40 and Cx43 predominantly localized to the same gap junction plaques (Fig. 1E-G). Confocal microscopic examination identified a few plaques that reacted only with the antibodies to one connexin (spots staining red or green only in merged image, Fig. 1G). These results are consistent with previous detection of Cx40 and Cx43 in gap junctions between mouse neonatal atrial myocytes [27]. We found that neonatal mouse ventricular myocytes showed intense Cx43 immunoreactivity; occasional cells showed a few spots of Cx40 staining at junctional plaques (data not shown).

The presence of Cx40 and of Cx43 in cell and tissue samples was also examined by immunoblotting (Fig. 2). N2a cells stably transfected with Cx40 or Cx43 (and untransfected cells) were blotted as positive (and negative) controls for detection of Cx40 or Cx43 (Figure 2A). The levels of Cx40 and Cx43 in the N2a transfectants (determined by comparison to standard curves generated using purified connexin fusion proteins) were Cx40, 128 ± 36 fmol/μg cellular protein, and Cx43, 74 ± 20 fmol/μg cellular protein (Fig. 2B). Cx43 was detected by immunoblotting in cultured atrial and ventricular myocytes and undissociated fresh frozen neonatal murine atrial and ventricular tissues (Fig. 2A, lower panel). In contrast, anti-Cx40 antibodies showed abundant reactivity with homogenates of atrial tissue and myocytes, weak reactivity with homogenates of ventricle, and no detectable reactivity with homogenates of isolated ventricular myocytes (Fig. 2A, upper panel). The atrial myocytes contained 404 ± 22 fmol/μg of Cx40 and 349 ± 62 fmol/μg of Cx43 (Fig. 2C); these levels did not differ significantly. Atrial tissue also contained similar levels of Cx40 and Cx43. Levels of both connexins were about half as much in the tissue samples as compared to the isolated cells; this difference may be due to the greater content of extracellular matrix proteins in the tissue samples. Limited analysis of quantitive blots showed that the abundunces of Cx40 and Cx43 were also very similar to each other in homogenates of adult atrium (not shown).

The isolated ventricular myocytes contained the highest levels of Cx43 (616 ± 78 fmol/μg), but no detectable Cx40 (<0.25 fmol of Cx40 per μg of cellular protein). Thus, while we cannot conclude that ventricular cells contain absolutely no Cx40 protein, the ratio of Cx40 to Cx43 in the neonatal mouse atrial myocytes and tissue was ~1:1. The ventricular tissue did contain a small amount of Cx40 (34 ± 4 fmol/μg) which could derive from the neonatal murine ventricular myocytes or from other cell types, such as the His-Purkinje system and the coronary endothelium [2,3,12,28,29]. Cx45 is also present in adult and neonatal myocytes from ventricle and atrium [2,28,29]. Therefore, we performed similar quantitive immunoblots, but we detected not more than 0.25 fmol/μg cellular protein in any sample (not shown) suggesting that Cx45 contributed only a very small fraction of the total connexins in any of these cells.

Real-time PCR analysis of RNA extracts from atrial and ventricular myocyte cultures confirmed high Cx43 atrial and ventricular gene expression levels with respective average delta cycle time (dCT) values of 0.71 ± 0.38 and 0.77 ± 0.26 (±S.D.; N = 3, 2) relative to GAPDH (Fig. 2D). Atrial Cx40 mRNA expression was slightly lower than Cx43, with a dCT value of 1.15 ± 0.25 and was barely detectable in ventricular myocyte culture samples (dCT = 5.4 ± 0.76). In an atrial myocyte culture derived from homozygous Cx40 knockout (Cx40KO) mice, Cx40 mRNA expression was not detectable (ND) and Cx43 expression levels were reduced (dCT = 1.7).

Functional Contributions of Cx40 and Cx43 to Atrial Gap Junctional Conductance

One direct way to assess the contribution of each connexin to the functional atrial gap junctional conductance (g_j) is to utilize the differential sensitivity of the cardiac connexins to inhibition by intracellular spermine [30]. For this purpose, 2 mM spermine was added unilaterally to one cell patch pipette and the fractional block of I_j was assessed using a Δ±10 mV, V_j pulse sequence [30,31] .

To demonstrate the differential sensitivity of the three mammalian myocardial connexins, Cx40, Cx43, and (Cx45), to spermine, the 2 mM spermine block assay was performed on N2a cells stably transfected with Cx40 or Cx43 or transiently transfected with Cx45 (Figure 3A). The maximum inhibition of g_j was 6 ± 6% for Cx43, 42 ± 10% for Cx45, and 80 ± 6% for Cx40 at V_j = +50 mV. Two way ANOVA analysis of V_j-dependent spermine inhibition indicated significant differences between these different connexins ($P<0.05$). These same procedures were applied to paired neonatal primary wild-type (wt) and homozygous Cx40 knockout (Cx40KO) mouse atrial and ventricular myocytes. The spermine block of wt ventricular g_j was significantly less than that of atrial g_j ($P<0.05$, two way ANOVA), and the maximum inhibition of g_j at +50 mV was 52 ± 12% and 19 ± 9% respectively for wt atrial and ventricular myocytes (Fig. 3B and C; see also Supplemental Material, Fig. S2). The atrial HL-1 cell line exhibited an intermediate degree of spermine block of 37 ± 10%. In contrast, the maximum inhibition of Cx40KO atrial and ventricular g_j at +50 mV were only 20 ± 14% and 3 ± 7% ($P<0.05$, two way ANOVA; Fig. 3B and C). There were no significant differences in the steady-state average g_j values among the connexin-N2a, atrial myocyte, or ventricular myocyte groups (see Suppmental Material Table S1). The lack of Cx40 expression in the Cx40KO atrial and ventricular cells and tissues was confirmed by immunoblot analysis (Fig. 3D). Taken together, these data based on the spermine block assay show that the fractional Cx40 contribution to the total cardiomyocyte g_j is approximately 40% in wt atrium.

V_j-dependent gating properties

Large myocardial V_j gradients can develop during slow, discontinuous conduction of cardiac action potentials, and V_j gradients equivalent to the amplitude of the ventricular cardiac action potential can induce phasic changes in g_j [15]. Therefore, we examined the dynamic and steady state gating properties of wt and Cx40KO mouse atrial gap junctions to detect possible functional differences. For the dynamic action potential voltage clamp experiments, cell 2 was continuously voltage clamped to a simulated atrial or ventricular cell resting potential while a sequence of 1/sec (basic cycle length, BCL = 1 sec) model atrial or ventricular action potentials was applied to cell 1 [22,24]. The atrial action potential waveform results in only minor normalized g_j (G_j) inactivation in wt and Cx40KO murine atrial gap junctions owing to a prominent early (phase 1) repolarization from a peak V_j of > 120 mV (Fig. 4A). To compare the inactivation of atrial gap junctions to their ventricular counterparts, we applied the ventricular model action potential to atrial and ventricular myocyte pairs. The average G_j from five experiments demonstrates that atrial gap junctions experience nearly 15% less inactivation and exhibit less facilitation; the overshoot of G_j during final (early phase 4) repolarization; than ventricular gap junctions (Figure 4B). The increased slope G_j (= $G_{max,rec}$) during the

falling phase of the V_j ramp is taken as a measure of the "facilitation" of G_j during the recovery phase [15,16]. The Cx40KO atrial G_j – time curve approached the wt ventricular G_j curve, indicating that the expression of Cx40 accounts for most, but not all, of the differences in gating between atrial and ventricular gap junctions.

The steady state G_j inactivation and recovery of atrial gap junctions was also examined using a slow (200 ms/mV) V_j ramp as previously described [15,16]. The wt atrial gap junctions displayed less inactivation and facilitation than their ventricular counterparts (Fig. 4C, D). The Cx40KO atrial steady state G_j–V_j inactivation curve was intermediate in form, and the recovery curve appeared similar to the wt atrial recovery curve with a slightly lower G_{min} value. The G_j – V_j curves were fit with a Boltzmann distribution (see Supplemental Materials), and the equation parameters are listed in SupplementaryTable S2. These results indicate that the V_j-dependent gating of atrial gap junctions is reduced in amplitude for both the inactivation and recovery phases whether in response to a cardiac action potential or to a slow, steady state V_j ramp.

Inactivation Kinetics

We further examined the inactivation process by evaluating the first order inactivation kinetics as a function of V_j. An example of the bi-exponential decay time constant determinations (τ_{fast} and τ_{slow}) for a wt and a Cx40KO atrial I_j recording is displayed in Figure 5A and B. The V_j-dependent closing rate constants ($\beta(V_j)$) for the fast and slow inactivation gates $k_{on,\ fast}$ and $k_{on,\ slow}$, were determined using the expression:

$$k_{on} = \left(1 - P_{open}\right) / \tau_{decay}. \quad \text{Eq. 2}$$

The wt atrial V_j-dependent fast and slow inactivation rates were well described by an exponential function with the values (in ms^{-1}) (Fig. 5C and D):

$$k_{on,\ fast} = (0.00701) \cdot \exp\left[\left(V_j - 60\right) / (18.6)\right] + (0.00586) \quad \text{Eq. 3}$$

and

$$k_{on,\ slow} = (0.00065) \cdot \exp\left[\left(V_j - 60\right) / (18.1)\right] + (0.00088). \quad \text{Eq. 4}$$

The V_j-dependent fast and slow on-rates for the Cx40KO atrial junctions were significantly faster at each examined V_j than their wt counterpart ($P<0.05$, two way ANOVA) and were best described by the following equations (in ms^{-1}):

$$k_{on,\ fast} = (0.010523) \cdot \exp\left[\left(V_j - 60\right) / (18.8)\right] + (0.00512) \quad \text{Eq. 5}$$

and

$$k_{on,\ slow} = (0.001427) \cdot \exp\left[\left(V_j - 60\right) / (18.6)\right] + (0.00078). \quad \text{Eq. 6}$$

These data provide the first demonstration that the V_j-dependence of the wt and Cx40KO gap junction atrial fast and slow inactivation rates are essentially the same, increasing e-fold approximately every 18 mV increase in V_j. These voltage constants are similar to those

previously reported for the wt fast and slow ventricular inactivation rates [16]. The fast and slow on-rates vary by a factor of 7 (e.g. τ_{fast} = 35 or 3 ms and τ_{slow} 244 o r16ms at 60 or 120 mV) for the Cx40KO and nearly 11 for the wt atrial gap junctions (e.g. τ_{fast} = 29 or 4 ms and τ_{slow} = 308 or 31 ms at 60 or 120 mV) according to these expressions. Cx40 gap junctions exhibit only slow inactivation that is similar to the slow inactivation component of Cx43 gap junctions [32,33].

We have previously modeled the dynamic gating of cardiac gap junctions based on our experimental description of the time- and V_j-dependent inactivation kinetics [15,16]. The "dynamic gap junction model" is defined in the Supplemental Appendix to this manuscript. The salient features of the model are that there are two (fast and slow) inactivation components, G_1^{t+dt} and G_2^{t+dt}, that possess identical voltage constants (**v**) for the V_j-dependent increase in the decay constants. There are also two recovery components, R_1^{t+1} and R_2^{t+1}, with different voltage constants (V_{R1} and V_{R2}) that are conserved between Cx40 and Cx43. All four components are solved according to the existing V_j during each time step (dt = 1 ms during patch clamp experiments) and the sum yields the function of G_j^{t+1} in time (= maximum of 1).

This dynamic gap junction model was used to fit the wt atrial G_j during the atrial and ventricular action potential waveforms. Since inactivation and facilitation were negligible during the atrial action potential (Fig. 4A), only the results using the ventricular action potential are presented in Figures 5E-F. The inactivation kinetics were the same as those described in Fig. 5B and C using a common voltage constant of 18.4 mV for both the fast and slow on-rates. In this example, G_{min1} and G_{min2} were assumed to be equal (0.42/2 = 0.21) and G_{max1} (= 0.33) and G_{max2} (= 0.22) were adjusted visually to provide a best fit of the time-dependent G_j inactivation curve using the Eq. 3&4 kinetic equations. The time-independent recovery processes were defined by the following parameters: R_{max1} = 0.4, R_{max2} = 1.25, V_{R1} = 47 mV, and V_{R2} = 1.6 mV. The only parameter changes required to fit the Cx40KO atrial G_j curve (Fig. 5F) were subsitution of the fast and slow inactivation kinetic equations (Eq. 5&6, Figs. 5B and C) and increasing A_{R2} to 1.54. The major differences between the dynamic gap junction models for the atrial and ventricular gap junctions are the slower atrial inactivation kinetics (ventricular A_2 = 0.00148) and the increased early recovery (ventricular V_{R1} = 22 mV) of the atrial G_j model relative to the previously described ventricular G_j model [15]. The time dependence of the wt atrial G_j in response to the canine atrial action potential could be modeled using this approach and required replacing the recovery process (Eq. A5) with a linear function. Determining how action potential morphology affects the magnitude and rate of the recovery process will require additional experimental evaluation, but the inactivation processes are well described by the existing time-and V_j-dependent functions with only minor modifications of the parameter values [15,16].

DISCUSSION

The principal purpose of this investigation was to assess quantitatively the contributions of Cx40 and Cx43 to the total atrial g_j and to determine how connexin co-expression alters the dynamic gating properties of atrial gap junctions relative to ventricular gap junctions. Our data show that atrial myocytes contain nearly equal amounts of Cx40 and Cx43; in contrast, in ventricular myocytes, Cx43 is as abundant, but Cx40 mRNA and protein are barely detectable or below the lower detection limit of our assays. A recent study provides evidence for interatrial differences in Cx40 expression that correlates with heterogeneities in conduction velocity, but the relative Cx40 and Cx43 mRNA or protein levels were not determined [12]. To determine the contribution of each connexin to the total atrial g_j, we took advantage of the knowledge that Cx40 gap junctions can be substantially inhibited by intracellular 2 mM spermine while Cx43 remains essentially unaffected [30]. This pharmacological assay revealed that slightly

more than half of atrial g_j was inhibited while slightly less than 20% of ventricular g_j was similarly blocked (Fig. 3).

Cx40 gap junction channels possess a ≥50% higher γ_j than the main open state of Cx43. Thus an equal contribution from Cx40 and Cx43 in the formation of homotypic homomeric gap junction channels would mean that at least 60% of the total atrial g_j is produced by Cx40 with the remainder being contributed by Cx43. Cx45 is also present in these cells [2,34], but its contribution to the total g_j is likely to be modest since our quantitative immunoblots suggest that its absolute abundance is very low (<1%) relative to Cx40 or Cx43. Similarly, RNA and Western blots performed by Vozzi et al. [34] show only very low levels of Cx45. The maximum inhibition of Cx40 g_j by spermine is 80%, so the 52 ± 12% block of atrial g_j by 2 mM spermine falls within the range of what would be expected from homotypic homomeric Cx40 and Cx43 gap junction channel populations in close proportions to their protein expression levels. The validity of this spermine block assay was assessed by performing the same procedures on atrial and ventricular myocyte cell pairs from homozygous Cx40KO hearts. The Cx40 gene deletion abolished the spermine block of ventricular gap junctions and reduced the block of atrial gap junctions to < 20%. The elimination of the ≈20% spermine block in ventricular gap junctions upon Cx40 gene deletion is consistent with the interpretation that a trace amount of Cx40 is expressed in our cultured neonatal murine ventricular myocytes. This interpretation is supported by our PCR results. The electrophysiological recordings and PCR assays may have a greater detection sensitivity than the immunoblots. Moreover, we have detected trace amounts of Cx40 protein by immunofluorescence between some of the cells in our cultures of neonatal ventricular myocytes (data not shown). Since Cx45 has an intermediate sensitivity to spermine, it might also account for a small percentage of the g_j block induced by 2 mM spermine in myocardial gap junctions. However, the lack of spermine inhibition of g_j in ventricular myocytes from Cx40KO hearts also suggests that the functional expression of Cx45, which is partially inhibited by spermine, is negligible. Limitations of the spermine block assay for assessing Cx40 contributions to cardiac gap junction conductance include the unknown effects of heteromeric or heterotypic combinations of Cx40 with Cx43, the relative sensitivity of Cx40 compared to Cx45, and the unknown cause for the continued presence of 20% block in homozygous Cx40KO atrial myocyte pairs.

The gating of atrial gap junctions during cardiac action potentials differs quantitatively from ventricular gap junctions. The V_j-dependent gating of atrial gap junctions is reduced in amplitude for both the inactivation and recovery phases whether in response to a cardiac action potential or to a slow, steady state V_j ramp. This functional gating difference may be due to the nearly equal coexpression of Cx40 and Cx43 in atrial gap junctions as compared to ventricular gap junctions where Cx43 pre-dominates. The Cx40 gene deletion resulted in an increase in the G_j inactivation rates, but did not completely convert the gating properties of atrial gap junctions to match those of ventricular gap junctions (Fig. 4). Thus, we hypothesize that factors in addition to Cx40 (perhaps, the presence of Cx45) alter the function of atrial gap junctions relative to their ventricular counterpart.

The inactivation kinetics for wt and Cx40 KO and atrial gap junctions were revealed to possess similar V_j-dependencies, increasing e-fold for approximately every 18 mV increase in V_j. This V_j-dependence is also similar voltage to what we recently reported for the fast and slow ventricular inactivation rates from wt ventricular gap junctions [16]. This implies that the V_j sensors for both fast and slow gates have the same valence, or that the same voltage sensor is involved in the closing of both fast and slow gates. The V_j sensor of gap junctions is proposed to reside on the connexin NT domain [35,36]. The fast V_j gating particle is thought to reside on the CT domain of Cx43 yet the CT domain interacts with second half of its own cytoplasmic loop (L2) domain, not the NT domain [37,38]. Cumulatively, these findings imply that the molecular bases for fast and slow inactivation components remain to be fully determined.

Action potential morphology will also influence the dynamic gating of cardiac gap junctions. Of particular importance is the magnitude and duration of the action potential derived peak and plateau V_j values. It was previously shown that the vast majority of cardiac g_j inactivation occurs when $V_j > 100$mV. Thus, the shorter the duration and the lower the amplutide of the action potential peak and plateau, the less G_j should inactivate. Our data using two different model action potentials, canine atrial and murine ventricular, demonstrate this point. This implies that regional differences in gap junction gating might occur on the basis of alterations in ion channel expression (e.g. ionic transient outward potassium (I_{TO}) currents) or function (e.g. ischemia) that affect action potential morphology [39,40]. We are presently investigating how varying action potential delays affect G_j inactivation.

The recovery from inactivation was also slightly altered in atrial gap junctions relative to their ventricular counterparts. The increased G_j during the declining phase of V_j was lower for atrial gap junctions. This facilitation of G_j above initial peak values was absent in HL-1 cells and Cx43-transfected N2a cells [15]. Thus, we propose that facilitation arises from a post-translational modification of Cx43, and possibly Cx40, protein that occurs in terminally differentiated myocytes but not in continuously dividing mammalian cell lines. Given the slight differences in inactivation and spermine block that were also observed in HL-1 cells, we conclude that primary cardiomyocyte cultures remain a better preparation for examining the possible role of gap junctions in cardiac action potential propagation and arrhythmogenesis. In summary, neonatal murine atrial myocytes express nearly identical amounts of Cx40 and Cx43 protein that contribute equally to functional gap junction coupling, the analysis of unilateral 2 mM sperrmine block provides a valid functional approach to the assessment of Cx40 contributions to cardiac gap junctional conductance, and quantitation of the V_j-dependent inactivation rates provide the basis for the development of realistic dynamic gap junction gating models as an investigative tool for further investigation into the role of cardiac g_j in action potential propagation and arrhythmogenesis.

Supplementary Material

Refer to Web version on PubMed Central for supplementary material.

Acknowledgments

This work was supported by HL-42220 to RDV, HL-59199 to ECB, AHA-SDG-0830018N to CWZ and performed with the technical assistance of Raymond Collins and Laura Coleman. The authors wish to thank Dr. Steven M. Taffet (SUNY Upstate Medical University) for his expert advice regarding the real-time PCR experiments and Dr. Viviana Berthoud (University of Chicago) for producing and contributing the Cx43 fusion protein.

REFERENCES

1. Kléber AG, Rudy Y. Basic mechanisms of cardiac impulse propagation and associated arrhythmias. Physiol Rev 2003;84:431–488.
2. Davis LM, Kanter HL, Beyer EC, Saffitz JE. Distinct gap junction phenotypes in cardiac tissues with disparate conduction properties. J Am Coll Cardiol 1994;24:1124–1132. [PubMed: 7930207]
3. Gros D, Jarry-Guichard T, Ten Velde I, de Maziere A, van Kempen MJ, Davoust J, Briand JP, Moorman AF, Jongsma HJ. Restricted distribution of connexin40, a gap junctional protein, in mammalian heart. Circ Res 1994;74:839–851. 1994. [PubMed: 8156631]
4. Kreuzberg MM, Söhl G, Kim J-S, Verselis VK, Willecke K, Bukuaskas FF. Functional properties of mouse connexin30.2 expressed in the conduction system of the heart. Circ Res 2005;96:1169–1177. [PubMed: 15879306]
5. Firouzi M, Ramanna H, Kok B, Jongsma HJ, Koeleman BP, Doevendans PA, Groenewegen WA, Hauer RN. Association of human connexin40 gene polymorphisms with atrial vulnerability as a risk factor for idiopathic atrial fibrillation. Circ Res 2004;95:e29–e33. [PubMed: 15297374]

6. Gollob DA, Jones DL, Krahn AD, Davis L, Liu X-Q, Veinot JP, Tang ASL, Stewart AFR, Tesson F, Klein GJ, Yee R, Skanes AC, Guiraudon G, Ebihara L, Bai D. Somatic mutations in the connexin 40 gene (GJA5). N Engl J Med 2006;354:2677–2688. [PubMed: 16790700]
7. Groenewegen WA, Firouzi M, Bezzina CR, Vliex S, van Langen IM, Sandkuji L, Smits JP, Hulsbeek M, Rook M, Jongsma HJ, Wilde AA. A cardiac sodium channel mutation cosegregates with a rare connexin40 genotype in familial atrial standstill. Circ Res 2003;92:14–22. [PubMed: 12522116]
8. Kirchhoff S, Nelles E, Hagendorff A, Krüger O, Traub O, Willecke K. Reduced cardiac conduction velocity and predisposition to arrhythmias in connexin40-deficient mice. Curr Biol 1998;8:299–302. [PubMed: 9501070]
9. Simon AM, Goodenough DA, Paul DL. Mice lacking connexin40 have cardiac conduction abnormalities characteristic of atrioventricular block and bundle branch block. Curr. Biol 1998;8:295–298. [PubMed: 9501069]
10. Hagendorff A, Schumacher B, Kirchhoff S, Luderitz B, Willecke K. Conduction disturbances and increased atrial vulnerability in Connexin40-deficient mice analyzed by transesophageal stimulation. Circulation 1999;99(11):1508–1515. [PubMed: 10086977]
11. Verheule S, van Batenburg CA, Coenjaerts FE, Kirchhoff S, Willecke K, Jongsma HJ. Cardiac conduction abnormalities in mice lacking the gap junction protein connexin40. J Cardiovasc Electrophysiol 1999;10:1380–1389. [PubMed: 10515563]
12. Leaf DE, Feig JE, Vasquez C, Riva PL, Yu C, Lader JM, Kontogeorgis A, Baron EL, Peters NS, Fisher EA, Gutstein DE, Morley GE. Connexin40 imparts conduction heterogeneity to atrial tissue. Circ Res 2008;103:1001–1008. [PubMed: 18599871]
13. Gutstein DE, Danik SB, Lewitton S, France D, Liu F, Chen FL, Zhang J, Ghodsi N, Morley GE, Fishman GI. Focal gap junction uncoupling and spontaneous ventricular ectopy. Am J Physiol Heart Circ Physiol 2005;289:H1091–1098. [PubMed: 15894579]
14. Gutstein DE, Morley GE, Vaidya D, Liu F, Chen FL, Stuhlmann H, Fishman GI. Heterogeneous expression of gap junction channels in the heart leads to conduction defects and ventricular dysfunction. Circ 2001;104:1194–99.
15. Lin X, Gemel J, Beyer EC, Veenstra RD. A dynamic model for ventricular junctional conductance during the cardiac action potential. Am J Physiol Heart Circ Physiol 2005;288:H1113–1123. [PubMed: 15513960]
16. Lin X, Zemlin C, Hennan JK, Petersen JS, Veenstra RD. Enhancement of ventricular gap junction coupling by rotigaptide. Cardiovasc Res 2008;79:416–426. [PubMed: 18430749]
17. Beblo DA, Wang H-Z, Beyer EC, Westphale EM, Veenstra RD. Unique conductance, gating, and selective permeability properties of gap junction channels formed by connexin40. Circ Res 1995;77:813–822. [PubMed: 7554128]
18. Veenstra RD, Wang HZ, Beblo DA, Chilton MG, Harris AL, Beyer EC, Brink PR. Selectivity of connexin-specific gap junctions does not correlate with channel conductance. Circ Res 1995;77:1156–1165. [PubMed: 7586229]
19. Musa H, Fenn E, Crye M, Gemel J, Beyer EC, Veenstra RD. Amino terminal glutamate residues confer spermine sensitivity and affect voltage gating and channel conductance of rat connexin40 gap junctions. J Physiol 2004;557:863–878. [PubMed: 15107469]
20. Luo CH, Rudy Y. A dynamic model of the cardiac ventricular action potential. I. Simulations of ionic currents and concentration changes. Circ Res 1994;74:1071–1096. [PubMed: 7514509]
21. Veenstra RD. Voltage clamp limitations of dual whole-cell gap junction current and voltage recordings. I. Conductance measurements. Biophys J 2001;80:2231–2247. [PubMed: 11325726]
22. Ramirez RJ, Nattel S, Courtemanche M. Mathematical analysis of canine atrial action potentials: rate, regional factors, and electrical remodeling. Am J Physiol Heart Circ Physiol 2000;279:H1767–1785. [PubMed: 11009464]
23. Kwong KF, Schuessler RB, Green KG, Laing JG, Beyer EC, Boineau JP, Saffitz JE. Differential expression of gap junction proteins in the canine sinus node. Circ Res 1998;82:604–612. [PubMed: 9529165]
24. Gong XQ, Shao Q, Lounsbury CS, Bai D, Laird DW. Functional characterization of a GJA1 frameshift mutation causing oculodentodigital dysplasia and palmoplantar keratoderma. J Biol Chem 2006;281:31801–31811. [PubMed: 16891658]

25. Beauchamp P, Yamada KA, Baertschi AJ, Green K, Kanter EM, Saffitz JE, Kléber AG. Relative contributions of connexins 40 and 43 to atrial impulse propagation in synthetic strands of neonatal and fetal murine cardiomyocytes. Circ Res 2006;99:1216–1224. [PubMed: 17053190]
26. Bastide B, Neyses L, Ganten D, Paul M, Willecke K, Traub O. Gap junction protein connexin40 is preferentially expressed in vascular endothelium and conductive bundles of rat myocardium and is increased under hypertensive conditions. Circ Res 1993;73:1138–1149. [PubMed: 8222085]
27. Yeh HI, Dupont E, Coppen S, Rothery S, Severs NJ. Gap junction localization and connexin expression in cytochemically identified endothelial cells of arterial tissue. J Histochem Cytochem 1997;45:539–550. [PubMed: 9111232]
28. Darrow BJ, Laing JG, Lampe PD, Saffitz JE, Beyer EC. Expression of multiple connexins in cultured neonatal rat ventricular myocytes. Circ Res 1995;76:381–387. [PubMed: 7859384]
29. Vossi C, Dupont E, Coppen SR, Yeh H-I, Severs NJ. Chamber related differences in connexin expression in the human heart. J Mol Cell Cardiol 1999;31:991–1003. [PubMed: 10336839]
30. Musa H, Veenstra RD. Voltage-dependent blockade of connexin40 gap junctions by spermine. Biophys J 2003;84:205–219. [PubMed: 12524276]
31. Lin X, Veenstra RD. Effect of transjunctional KCl gradients on the spermine inhibition of connexin40 gap junctions. Biophys J 2007;93:483–495. [PubMed: 17468172]
32. Lin X, Crye M, Veenstra RD. Regulation of connexin43 gap junctional conductance by ventricular action potentials. Circ Res 2003;93:e63–e73. [PubMed: 12946947]
33. Lin X, Veenstra RD. Action potential modulation of connexin40 gap junctional conductance. Am J Physiol Heart Circ Physiol 2004;286:H1726–1735. [PubMed: 14693688]
34. Vossi C, Dupont E, Coppen SR, Yeh H-I, Severs NJ. Chamber related differences in connexin expression in the human heart. J Mol Cell Cardiol 1999;31:991–1003. [PubMed: 10336839]
35. Bukauskas FF, Verelis VK. Gap junction channel gating. Biochim Biophys Acta 2004;1662:42–60. [PubMed: 15033578]
36. Verselis VK, Ginter CS, Bargiello TA. Opposite voltage gating polarities of two closely related connexins. Nature 1994;368:348–351. [PubMed: 8127371]
37. Duffy HS, Sorgen PL, Girvin ME, O'Donnell P, Coombs W, Taffet SM, Delmar M, Spray DC. pH-dependent intramolecular binding and structure involving Cx43 cytoplasmic domains. J Biol Chem 2002;277:36706–36714. [PubMed: 12151412]
38. Moreno AP. Biophysical properties of homomeric and heteromultimeric channels formed by cardiac connexins. Cardiovasc Res 2004;62:276–286. [PubMed: 15094348]
39. Schram G, Pourrier M, Melnyk P, Nattel S. Differential distribution of cardiac ion channel expression as a basis for regional specialization in electrical function. Circ Res 2002;90:939–950. [PubMed: 12016259]
40. Sicouri S, Antzelevitch C. A subpopulation of cells with unique electrophysiological properties in the deep subepicardium of the canine ventricle: the M cell. Circ Res 1991;68:1729–1741. [PubMed: 2036721]

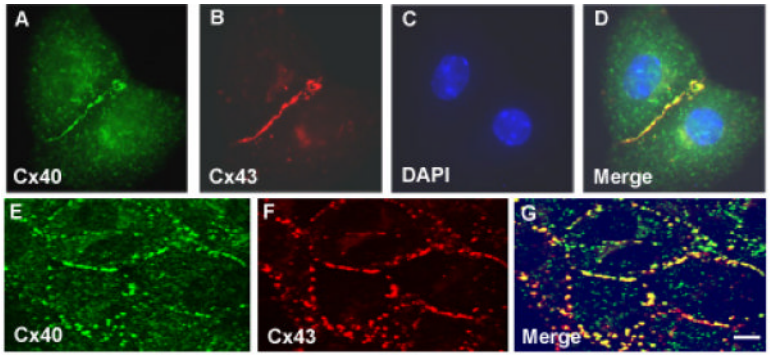

Figure 1.

Immunofluorescent localization of Cx40 and Cx43 in neonatal mouse atrial cultures. **A-D,** atrial myocyte cell pair showing immunolocalization of Cx40 (green in A), Cx43 (red in B). Nuclei were identified by staining with DAPI (blue in C, D). **E-G,** confocal images of an atrial myocyte cell culture immunostained for Cx40 (green in E) and Cx43 (red in F). Merged images are shown in the right panel (G) where overlap appears yellow. In atrial myocytes Cx40 and Cx43 localize to gap junction plaques and show substantial overlap, however there are some spots stained with only one color suggesting discrete domains of each connexin. Bar represents 6.25 μm for A-D, 5 μm for E-G.

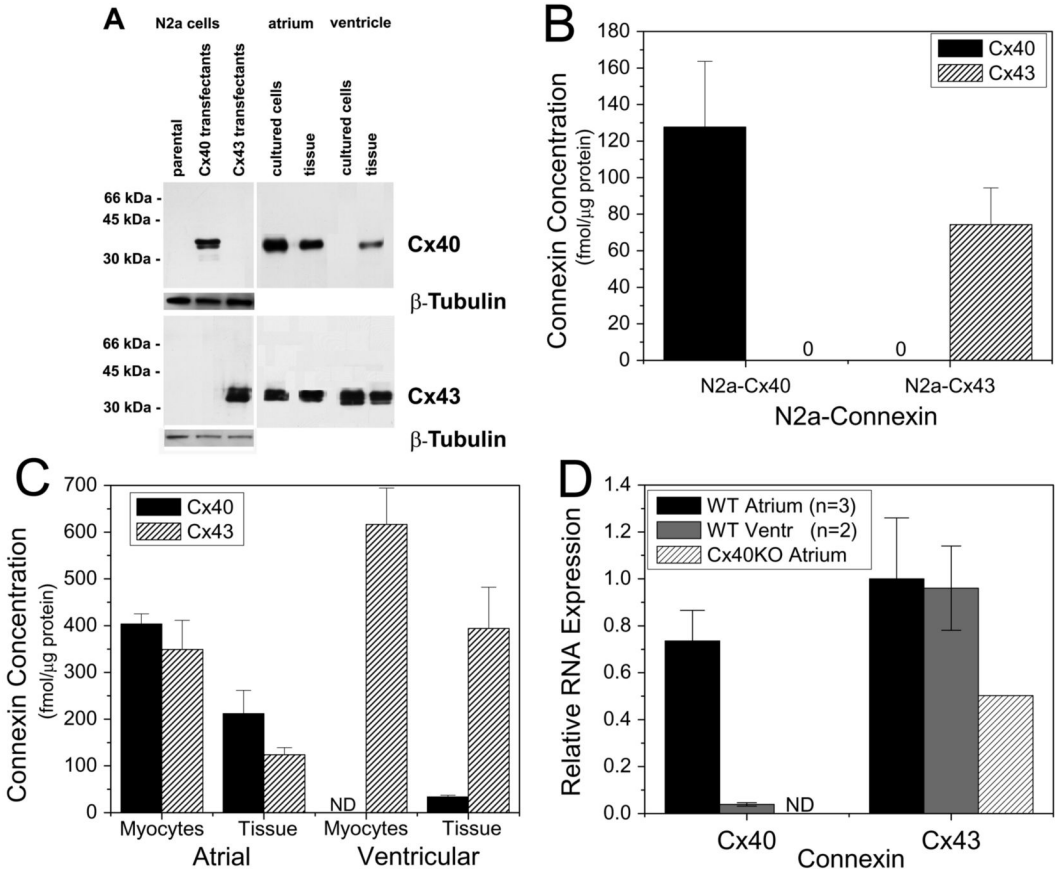

Figure 2.

Immunoblot analysis of Cx40 and Cx43 in cultured cells or fresh frozen atrial and ventricular tissues from neonatal mice. Whole cell lysates (for Cx40 detection: 5 μg protein from N2a cells and ventricular samples, 1 μg protein from atrial samples; for Cx43 detection: 2 μg protein for all samples except atrial tissue when 5 μg protein was used) were resolved by SDS-PAGE, transferred to membranes, and blotted with anticonnexin or anti β-tubulinantibodies. **A,** Photograph of a representative immunoblot. Migration of molecular weight markers is indicated to the left of the blot. Exposure times differ for the parts of the figure containing N2a cells and heart samples. ß-tubulin was used as a loading control for N2a cells. **B,** Absolute abundances of Cx40 and Cx43 in N2a transfectants. Bars represent the mean value ±SEM based on 3 experiments. **C,** Absolute abundances of Cx40 and Cx43 in mouse neonatal heart (isolated cells and tissue homogenates). Blots also contained serial dilutions of bacterially expressed Cx40 or Cx43 fusion proteins (See Supplementary Fig. S1). Reaction products were quantified using a phosphoimager and abundances of Cx40 and Cx43 were determined by comparison to these standard curves. Each bar represents the mean value ±SEM based on n number of experiments; for atrial myocytes Cx40 n=4, Cx43 n=3, atrial tissue Cx40 n=3, Cx43 n=4, ventricular myocytes Cx40 n=4, Cx43 n=4, ventricular tissue Cx40 n=4, Cx43 n=5. **D,** Real-time PCR analysis of Cx40 and Cx43 gene expression in cultured atrial and ventricular myocytes. Atrial Cx40 expression was slightly lower than wild-type (WT) atrial or ventricular Cx43 expression, was barely detectable in WT ventricular myocyte cultures, and was absent from homozygous Cx40 knockout (Cx40KO) cultured atrial myocytes (ND = Not Detectable). Cx40KO atrial Cx43 gene expression was reduced relative to WT samples. Relative expression levels were calculated based on the differences in the cycle times (dCT) required for product amplification (see Methods for details).

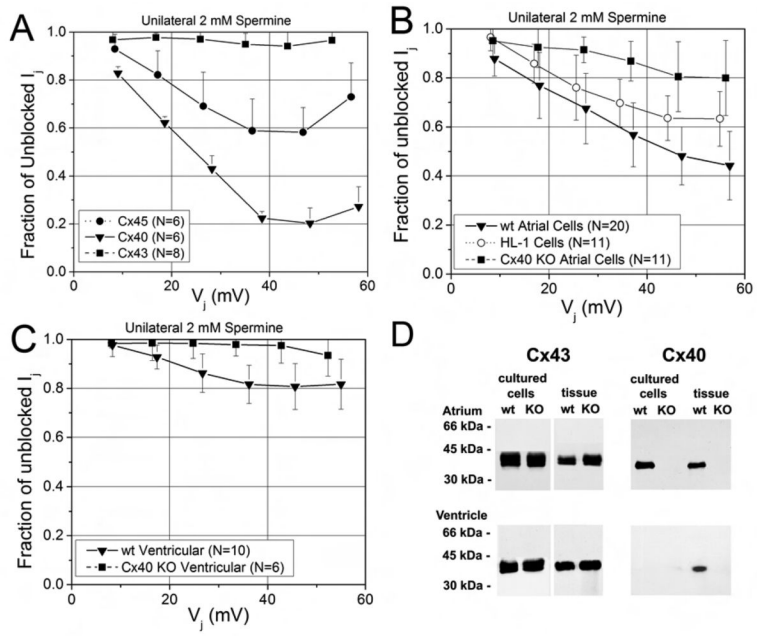

Figure 3.

Spermine inhibition of steady-state cardiac junctional conductances. **A,** The fraction of unblocked I_j (= $I_{j(KCl + 2mM\ spermine)}/I_{j(KCl)}$) from homptypic N2a cell pairs transfected with rat Cx40(▼), Cx43 (■), or mouse Cx45 (●). Symbols are the mean ± s.d. for N number of experiments. **B,** The fraction of unblocked I_j from wt atrial (▼), Cx40KO atrial (■), and HL-1 (○) myocyte cell pairs. **C,** The fraction of unblocked I_j from wild-type ventricular (▼) and Cx40KO ventricular (■) myocyte cell pairs. The percent inhibition by 2 mM spermine was 16-fold higher for Cx40 than Cx43 gap junctions and 2.5 times greater in wt atrial compared to ventricular gap junctions. The germline deletion of Cx40 reduced atrial and ventricular gap junction spermine block to ≤ 20% and ≤ 10% respectively. **D,** Immunoblot analysis of Cx43 and Cx40 in cultured cells or fresh frozen atrial and ventricular tissues from neonatal wild type or Cx40 knock-out mice. Cx43 and Cx40 were detected by immunoblotting of whole cell or tissue homogenates (for the detection of Cx43: 10 μg of protein for tissues, 5 μg of protein for cells; for the detection of Cx40: 30 μg of protein for all samples except cells from atrium when 15 μg of protein was used). Immunoblot analysis shows no detectable Cx40 expression in Cx40KO atrial and ventricular cells and tissues.

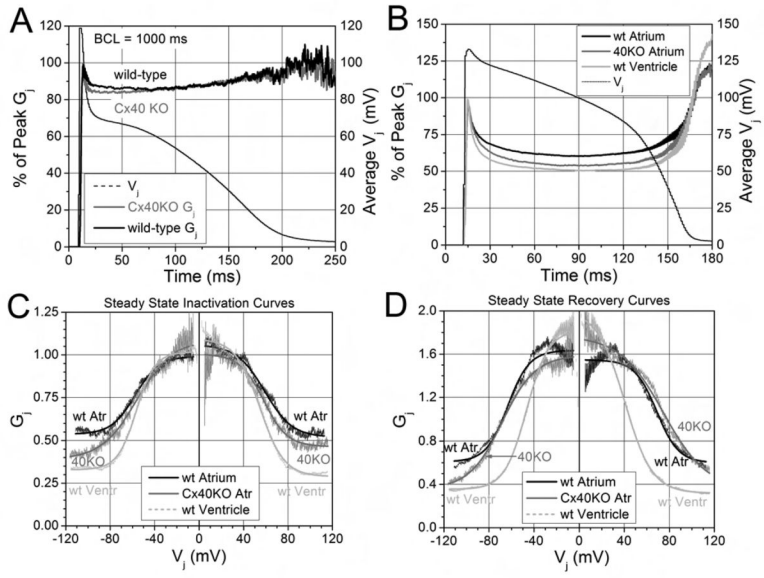

Figure 4.

V_j-dependent gating properties of atrial gap junctions. **A,** Gating of wt and Cx40KO atrial G_j during the canine atrial action potential. The spike morphology of BCL = 1 sec atrial action potential produced only 10-20% inactivation and recovery of atrial G_j. Cx40KO atrial gap junctions exhibited more inactivation than their wt counterpart. **B,** Comparison of the gating of wt (black) and Cx40KO (gray) atrial G_j to wt ventricular (light gray) G_j during the BCL =1 sec ventricular action potential. The higher amplitude and duration of the the peak and plateau V_j produces dramatically more (33-50%) inactivation and facilitated recovery of G_j. Atrial G_j inactivation was less than in the ventricle, but was enhanced by the deletion of Cx40. **C,** Steady state $G_j - V_j$ inactivation curves exhibit a similar relative profile for wt atrial, Cx40KO atrial, and wt ventricular G_j due to the dereasing half-inactivation voltage ($V_{½}$) and minimum G_j (G_{min}) values of the three Boltzmann distributions (see Table S2). **D,** The steady-state recovery $G_j - V_j$ curves exhibit less facilitation of wt or Cx40KO atrial G_j that commences at higher V_j values than in the wt ventricle.

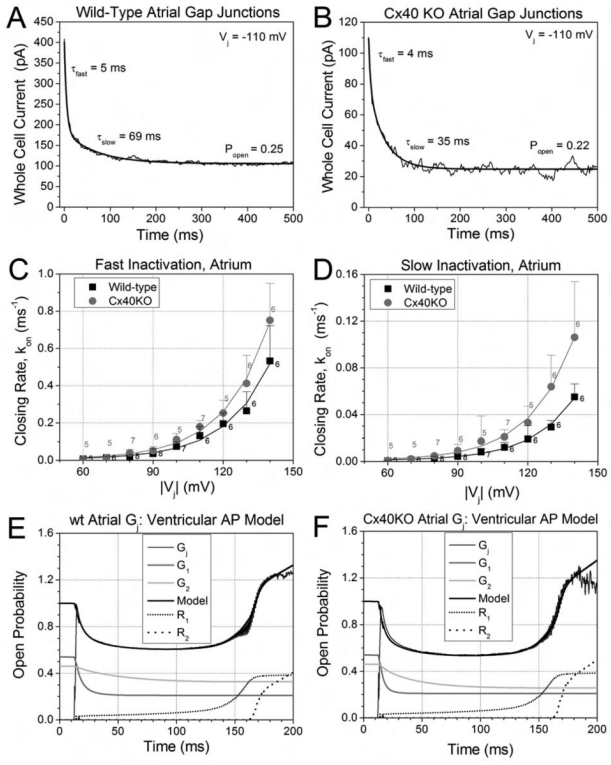

Figure 5.

Inactivation kinetics and dynamic action potential model of atrial gap junctions. **A,** An example of a whole cell (I_2) current during a voltage clamp step to −110 mV from a single wt atrial myocyte experiment. The fast and slow decay time constants (τ_{fast} and τ_{slow}) were determined by exponential curve fitting of the I_j trace. **B,** A similar example of the decay time constant (τ) curve-fitting and open probability (P_{open}) measurements for a Cx40KO atrial I_j recording. **C,** The average fast inactivation rates ($k_{on,\ fast}$ mean ± s.d., n = 5-8), for wt and Cx40KO atrial G_j increased exponentially with V_j (voltage constant of 18.6-8 mV). **D,** The average slow inactivation rates ($k_{on,\ slow}$) for wt and Cx40KO atrial G_j similarly increased exponentially with a V_j constant (ν) of 18.1-6 mV. **E,** Dynamic gap junction model fit of time-dependent wt atrial G_j curve during the BCL = 1 sec ventricular action potential using the kinetic inactivation parameters from panels C and D. The wt atrial G_j model is similar to the previously described ventricular G_j model except that the inactivation kinetics were slower and the early recovery commences sooner [15]. **F,** Dynamic gap junction model fit of time-dependent Cx40KO atrial G_j curve during the same model ventricular action potential. The Cx40KO atrium had faster inactivation kinetics and slightly more late recovery (R_2) than wt atrial G_j